1-1-2014

Dispersive shock waves in colloids with temperature dependent compressibility

Amirah Azmi
aa438@uowmail.edu.au

Timothy R. Marchant
University of Wollongong, tim@uow.edu.au

Dispersive shock waves in colloids with temperature dependent compressibility

Abstract

The formation of a dispersive shock wave in a colloidal medium, due to an initial jump in the light intensity, is studied. The compressibility of the colloidal particles is modeled using a series in the particle density, or packing fraction, where the virial coefficients depend on the particle interaction model. Both the theoretical hard disk and sphere repulsive models, and a model with temperature dependent compressibility, are considered. Experimental results for the second virial coefficient show that it is temperature dependent and that the particle interactions can be either repulsive or attractive. These effects are modeled using a power-law relationship. The governing equation is a focusing nonlinear Schrödinger-type equation with an implicit nonlinearity. The initial jump is resolved via a dispersive shock wave which forms before the onset of modulational instability. A semi-analytical solution is developed for the one-dimensional line bore case which predicts the amplitude of the solitary waves which form in the dispersive shock wave. The solitary wave amplitude versus jump height diagrams can exhibit three different kinds of behaviors. A unique solution, an S-shaped solution curve and multiple solution branches where the upper branch has separated from the lower branches. A bifurcation from the low to the high power branch can occur for many parameter choices as the amplitude of the initial jump increases. The effect of temperature on the evolution of the bore, the amplitude of the solitary waves and the bifurcation patterns are all discussed and the semi-analytical solutions are found to be very accurate.

Keywords

dispersive, shock, colloids, compressibility, waves, dependent, temperature

Disciplines

Engineering | Science and Technology Studies

Publication Details

Azmi, A. & Marchant, T. (2014). Dispersive shock waves in colloids with temperature dependent compressibility. Journal of Nonlinear Optical Physics and Materials, 23 (4), 1-22.

Dispersive shock waves in colloids with temperature dependent compressibility

A. Azmi
School of Mathematical Science,
Universiti Sains Malaysia,
11800 USM Penang,
Malaysia
amirah_azmi@hotmail.com

T.R. Marchant
School of Mathematics and Applied Statistics,
The University of Wollongong,
Wollongong, 2522, N.S.W., Australia.
tim_marchant@uow.edu.au

Abstract

The formation of a dispersive shock wave in a colloidal medium, due to an initial jump in the light intensity, is studied. The compressibility of the colloidal particles is modelled using a series in the particle density, or packing fraction, where the virial coefficients depend on the particle interaction model. Both the theoretical hard disk and sphere repulsive models, and a model with temperature dependent compressibility, are considered. Experimental results for the second virial coefficient show that it is temperature dependent and that the particle interactions can be either repulsive or attractive; these effects are modelled using a power law relationship. The governing equation is a focusing nonlinear Schrödinger-type equation with an implicit nonlinearity. The initial jump is resolved via a dispersive shock wave which forms before the onset of modulational instability. A semi-analytical solution is developed for the one dimensional line bore case which predicts the amplitude of the solitary waves which form in the dispersive shock wave. The solitary wave amplitude versus jump height diagrams can exhibit three different kinds of behaviours; an unique solution, an S-shaped solution curve and multiple solution branches where the upper branch has separated from the lower branches. A bifurcation from the low to the high power branch, can occur for many parameter choices, as the amplitude of the initial jump increases. The effect of temperature on the evolution of the bore, the amplitude of the solitary waves and the bifurcation patterns are all discussed and the semi-analytical solutions are found to be very accurate.

keywords solitary waves, dispersive shock waves, nonlocal optical media, conservation laws

1 Introduction

The development of dispersive shock waves in colloidal media is considered using a nonlinear Schrödinger (NLS)-type equation with implicit nonlinearity, where the nanoparticle interactions, or compressibility, are described by a series form. Dispersive shock waves (DSW) in colloidal media are subject to modulational instability (MI) and do not persist at long length scales. However DSW's can occur in focusing media over experimental length scales, in both a focusing photorefractive medium[1] and a nematic liquid crystal medium[2]. Hence, it is of interest as to whether experimentally observable DSW's also occur in colloidal media.

The formation of a DSW in a nematic liquid crystal medium was considered[3]. In such media the DSW persists for experimentally relevant propagation distances due to nonlocality delaying the onset of MI. Semi-analytical solutions for one dimensional line bores and two dimensional circular bores were considered. The theoretical predictions were in excellent agreement with numerical solutions of the governing equations. A DSW in a colloidal media was also examined[4] by using the Carnahan Starling (CS) hard sphere particle interaction model. They found that the results are dependent on the background packing fraction with three different types of solitary wave amplitude versus jump height diagrams possible.

The compressibility of colloidal particles can be defined in series form as a function of the packing fraction. The nature of the interactions between the colloidal nanoparticles defines the virial coefficients of the perturbation series. The classical theoretical repulsive interaction models are the hard disk (HD) model, valid in one dimension, and hard sphere (HS) model, valid in two dimensions. Experimental results for the second virial coefficient, which describes the leading density dependent correction to the ideal gas law, indicate that it can be modelled by a power law[5].

This paper considers the evolution a colloidal DSW, where the compressibility function has a series form. We use the semi-analytical colloidal solitary wave solutions[6], together with uniform soliton theory to obtain semi-analytical expressions for the amplitude of the solitary waves generated by the DSW. The (1+1)-D HS and HD models together with the temperature dependent results are used to understand the colloidal (1+1)-D line DSW, such as its behaviour for different background packing fractions and the bifurcation patterns that develop. The semi-analytical solutions are shown to be accurate, in comparison with the numerical solutions.

2 Governing equations and modulation equations

The NLS-type equation that governs the nonlinear propagation of the beam through a colloidal suspension[7], is

$$i\frac{\partial u}{\partial z} + \frac{1}{2}\nabla^2 u + (\eta - \eta_0)u = 0, \quad |u|^2 = g(\eta) - g_0, \tag{1}$$
$$g(\eta) = \ln(\eta) + 2B_2\eta + \frac{3}{2}B_3\eta^2 + \cdots, \quad g(\eta_0) = g_0,$$

where u is the electric field envelope, η is the packing fraction of the colloid particles, and η_0 is the background packing fraction. The governing equation is independent of time t but the propagation variable z plays a time like role. Physically it is assumed that the light beam causes the colloidal particles to drift towards the region of higher light intensity, due to electrostriction. Also, the colloidal particles have a higher refractive index than the background liquid medium. So when an optical beam passes through the medium the optical gradient force acts against particle diffusion, increasing the concentration of colloidal particles and hence the refractive index, in regions of higher light intensity, allowing self-focusing to occur.

Equation (2) and (3) below describe the compressibility series for the HS and HD models. For both models typically five or six series terms are needed, to obtain equivalent results to the CS and SPT theories, at large packing fractions. Here we use the seven term series,

$$Z = 1 + 4\eta + 10\eta^2 + 18\eta^3 + 28\eta^4 + 40\eta^5 + 54\eta^6 + \cdots, \tag{2}$$
$$Z = 1 + 2\eta + 3\eta^2 + 4\eta^3 + 5\eta^4 + 6\eta^5 + 7\eta^6 + \cdots, \tag{3}$$

where the coefficients in equation (2) are obtained from Table 3[8] while (3) is from Table I[9]. We also develop a temperature dependent model by using known experimental results as a guide. The power law

$$B_2 = b - \frac{a}{T^{\beta+1}}, \tag{4}$$

is used to model the temperature dependence of the second virial coefficient[8]. As the non-dimensional temperature T varies, the second coefficient B_2 can change from positive to negative, which changes the particle interaction forces from repulsive to attractive. To model temperature effects we use the HD coefficients (3) but with (4) as the second virial coefficient where $B_2 = 2 - \frac{100}{T}$. So in the limit as the temperature becomes large, the model approaches the repulsive HD one, as $B_2 \to 2$. This choice of B_2 allows us to explore the effects on the DSW as the temperature changes and the interaction forces vary between repulsive and attractive cases.

The colloid equations (1) have the Lagrangian formulation

$$L = i(u^* u_z - u_z{}^*) - |\nabla u|^2 + 2(\eta - \eta_0)|u|^2 - 2\eta\ln\eta + 2\eta_0\ln\eta_0 \tag{5}$$
$$+2(\eta - \eta_0)(1 + g_0) - 6\eta - 2B_2\eta^2 - B_3\eta^3 + 6\eta_0 + 2B_2\eta_0^2 + B_3\eta_0^3 + \cdots,$$

where the asterisk superscript denotes the complex conjugate. We look for solitary wave solutions for the (1+1)-D form of the colloid equations (1), which are functions of the two spatial coordinates, x and z, where z plays the time-like role. We are only concerned here with steady-state envelope solitary waves (where the envelope is only a function of x) and we choose trial functions for the electric field and colloid packing fraction in (1+1)-D as

$$u(x,z) = a\ \mathrm{sech}\frac{x}{w}e^{i\sigma z}, \quad \eta(x) = \eta_0 + \alpha\ \mathrm{sech}^2\frac{x}{\beta}. \tag{6}$$

The choice of trial functions allows the amplitude and width to vary explicitly[10]. The solitary wave (6) can be chosen as stationary without loss of generality, as a non-zero velocity can be scaled out of the equations. The electric field component of the solitary wave is based on the NLS soliton sech profile. The form for the packing fraction η is chosen as a sech^2 profile as η is a function of the light intensity $|u|^2$ and $\eta \to \eta_0$ far from the light pulse. The parameters in equation (6) are the amplitudes a and α while the widths are w and β and σ is the propagation constant of the solitary wave. As the full details are available[6] so only the final equations are presented here

$$\begin{aligned}
&3\alpha w(\Omega_1 - w\Omega_{1w}) - 1 = 0, \quad \sigma = -\frac{1}{2w^2} + \frac{\alpha}{w}(2\Omega_1 - w\Omega_{1w}), \qquad (7)\\
&4a^2\alpha(\Omega_1 - \beta\Omega_{1\beta}) - 4\beta(\alpha\Theta_{1\alpha} - \Theta_1) - \frac{8}{3}B_2\alpha^2\beta - 4B_3\eta_0\alpha^2\beta\\
&-\frac{32}{15}B_3\alpha^3\beta = 0,\\
&\alpha a^2\Omega_{1\beta} - 4\Theta_1 + 4\alpha(1+g_0) - 8B_2\alpha\eta_0 - \frac{8}{3}B_2\alpha^2 - 6B_3\eta_0^2\alpha\\
&-4B_3\eta_0\alpha^2 - \frac{16}{15}B_3\alpha^3 = 0.
\end{aligned}$$

which describe a two-parameter family of solitary waves.

3 Uniform soliton theory and the dispersive shock wave

We investigate the development of a DSW for the focusing colloidal equation (1) by looking at an IVP with the jump initial condition

$$u = \begin{cases} a_m e^{ikx}, & x < 0, \\ 0, & x > 0, \end{cases} \quad \eta = \begin{cases} \eta_m, & x < 0, \\ \eta_0, & x > 0, \end{cases} \tag{8}$$

where a_m is the amplitude of the jump in electric field and k is the wavenumber of the continuous wave. The first of (8) is the jump in the electric field amplitude $|u|$ and there also exists a corresponding jump in the packing fraction, as in the second of (8). The correlation between these two jumps is linked by the state

equation, ${a_m}^2 = g(\eta_m) - g_0$. In $x < 0$, the initial condition is always a continuous wave and there is nothing in $x > 0$.

We assume that the bore generates a train of solitary waves of uniform amplitude, given by (1). In order to obtain an approximation for the amplitude of the solitary waves, we use uniform soliton theory[11, 12]. The mass conservation equation of (1) is

$$i\frac{\partial}{\partial z}|u|^2 + \frac{1}{2}\frac{\partial}{\partial x}(u^* u_x - u {u_x}^*) = 0, \tag{9}$$

and the energy equation is given by

$$\begin{aligned} & i\frac{\partial}{\partial z}[|u_x|^2 - 2(\eta - \eta_0)|u|^2 + 2\eta\ln\eta + 2\eta_0\ln\eta_0 - 2(\eta - \eta_0)(1 + g_0) \\ & +6\eta + 2B_2\eta^2 + B_3\eta^3 - 6\eta_0 - 2B_2\eta_0^2 - B_3\eta_0^3 + \cdots] \\ & +\frac{1}{2}\frac{\partial}{\partial x}[{u_x}^* u_{xx} - u_x u_{xx}^* - 2(\eta - \eta_0)(u^* u_x - u {u_x}^*)] = 0. \end{aligned} \tag{10}$$

We integrate the conservation laws from $x = -\infty$ to $x = \infty$. As the boundary condition at $x = -\infty$ is non-zero, as described by (8), the x derivative terms are non-zero at $x = -\infty$. Integrating the conservation equations then gives

$$\begin{aligned} & \frac{d}{dz} < M >= k{a_m}^2, \quad \frac{d}{dz} < H >= k{a_m}^2[k^2 - 2(\eta_m - \eta_0)], \quad \text{where} \\ & M = |u|^2, \quad H = [|u_x|^2 - 2(\eta - \eta_0)|u|^2 + 2\eta\ln\eta + 2\eta_0\ln\eta_0 \\ & -2(\eta - \eta_0)(1 + g_0) + 6\eta + 2B_2\eta^2 + B_3\eta^3 - 6\eta_0 - 2B_2\eta_0^2 \\ & -B_3\eta_0^3 + \cdots], \quad < . >= \int_{-\infty}^{\infty} . \ \mathrm{d}x. \end{aligned} \tag{11}$$

From equation (11), we see that the conservation laws depend on k, which is the wavenumber of the initial condition. We then take the ratio of the two equations in (11) in the limit of $k \to 0$, and integrate, giving

$$< H > +2(\eta_m - \eta_0) < M >= 0. \tag{12}$$

Equation (12) is the condition that describes, for small wavenumber, the mass to energy ratio generated by the initial condition. We assume that solitary waves generated by the bore have this same mass to energy ratio. However, for NLS-type equations, the solitary waves amplitude is independent of wavenumber, so (12) applies for all wavenumbers[3]. We now use the semi-analytical expression for a single colloidal solitary wave (6) which gives

$$\begin{aligned} & < M >= 2a^2 w, \quad < H >= P, \quad \text{where} \\ & P = \frac{2}{3}\frac{a^2}{w} - 4\alpha a^2\Omega_1 - 4\alpha\beta(1 + g_0) + 4\beta\Theta_1 + 8B_2\alpha\beta\eta_0 + \frac{8}{3}B_2\alpha^2\beta \\ & +6B_3{\eta_0}^2\alpha\beta + 4B_3\eta_0\alpha^2\beta + \frac{16}{15}B_3\alpha^3\beta + 2(\eta_m - \eta_0)(2a^2 w). \end{aligned} \tag{13}$$

Substituting (13) into (12) then gives the transcendental equation

$$\frac{2}{3}\frac{a^2}{w} - 4\alpha a^2\Omega_1 - 4\alpha\beta(1+g_0) + 4\beta\Theta_1 + 8B_2\alpha\beta\eta_0 + \frac{8}{3}B_2\alpha^2\beta$$
$$+6B_3{\eta_0}^2\alpha\beta + 4B_3\eta_0\alpha^2\beta + \frac{16}{15}B_3\alpha^3\beta + 4a^2w(\eta_m - \eta_0) = 0. \qquad (14)$$

From equation (14), together with the transcendental equations (7) for (1+1)-D solitary waves, we then obtain the amplitude a and α together with the width w and β of the electric field and packing fraction solitary waves in the DSW. These solitary wave properties are given in terms of the initial jump a_m. It is important to note that the wavenumber can be non-zero because the waves can move to the right in the speed of $V = k$, but the value of the wavenumber does not effect the amplitude or number of the waves in the dispersive shock wave.

4 The (1+1)-D line DSW

Bifurcation patterns (a versus a_m graphs) and the evolution of the DSW, at different background packing fraction values, are considered. For (1+1)-D colloids, the HD model is geometrically appropriate but the HS model has been widely used in previous studies. So, both the HS and HD models are examined, to see what differences occur. A model with temperature dependent compressibility is also used. The numerical solutions of the colloidal equations (1) will be compared with the semi-analytical solutions developed for the (1+1)-D line DSW. We use a hybrid Runge-Kutta finite difference scheme for the numerical solutions.

4.1 Hard sphere and hard disk models

Figure 1 shows the dispersive shock height, a_m at the bifurcation point versus the background packing fraction η_0 as described by (7), (14) and $\frac{da_m}{da} = 0$ for the (a) HS and (b) HD models. The uniform soliton theory is presented. If a solitary wave amplitude a versus shock height a_m diagram is considered, then $\frac{da_m}{da} = 0$ is the condition for a bifurcation point to occur in this diagram. The figure shows that for any value of $\eta_0 > 5.65 \times 10^{-3}$ for the HS model and $\eta_0 > 10.5 \times 10^{-3}$ for the HD model, no bifurcation point exists. This indicates that a single, stable, a versus a_m solution branch will occur beyond these values of η_0. These are the parameter values that separate the bi-stable and mono-stable regimes for the solitary wave solution for the (1+1)-D colloids[7, 13]. We also get two other types of a versus shock height a_m diagrams. The first type occurs for $3.96 \times 10^{-3} < \eta_0 < 5.65 \times 10^{-3}$ for the HS model and $7.4 \times 10^{-3} < \eta_0 < 10.5 \times 10^{-3}$ for the HD model, where S-shaped response curves are obtained. This kind of S-shaped response curve is similar to the multiple steady-state response curve seen in combustion theory for reaction-diffusion systems with an Arrhenius law. In combustion theory, an S-shaped response curve is considered a classical result; it has two turning points along the bifurcation curve. If the

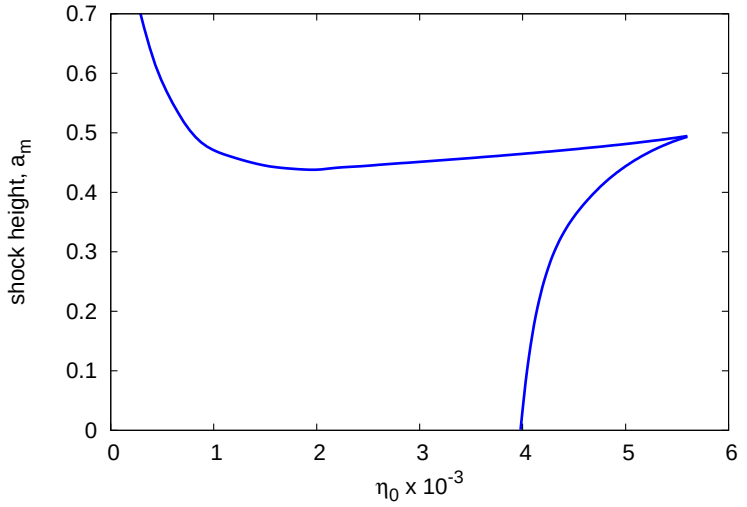

(a)

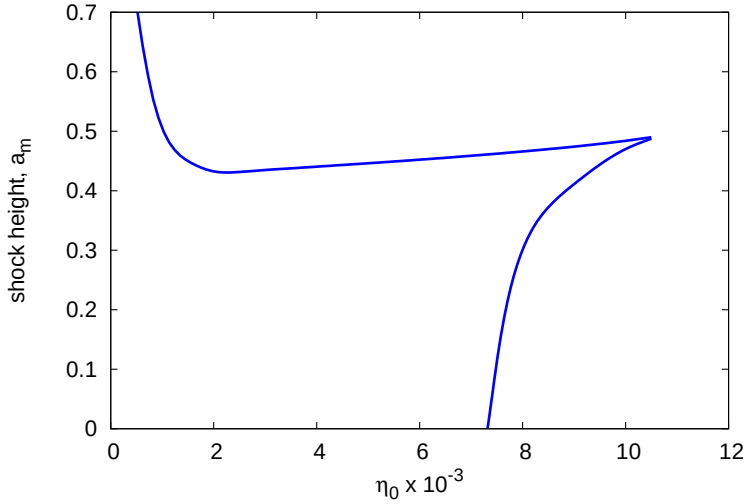

(b)

Figure 1: The dispersive shock height, a_m, at the bifurcation point, versus the background packing fraction η_0 for (a) HS and (b) HD models.

solution jumps from the low temperature to the high temperature branch, this will cause a thermal runaway[14, 15]. However it is very unusual to observe this behaviour in optical solitary wave applications. For $\eta_0 < 3.96 \times 10^{-3}$ in the HS model and $\eta_0 < 7.4 \times 10^{-3}$ in the HD model, we get the three solution branches,

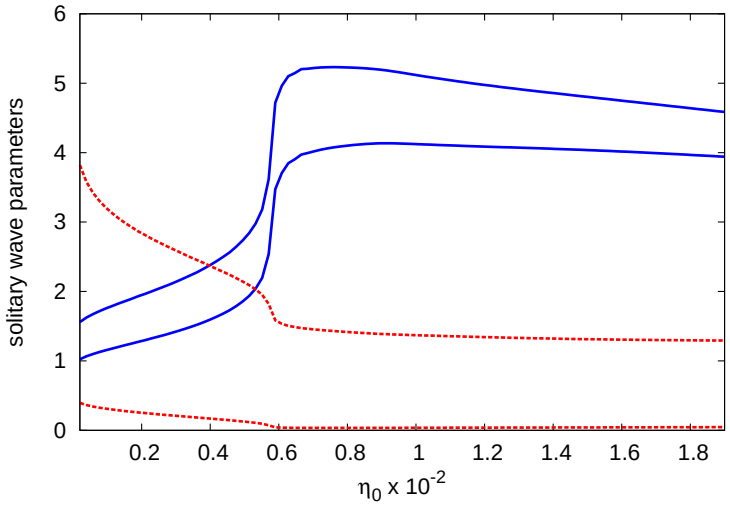

(a)

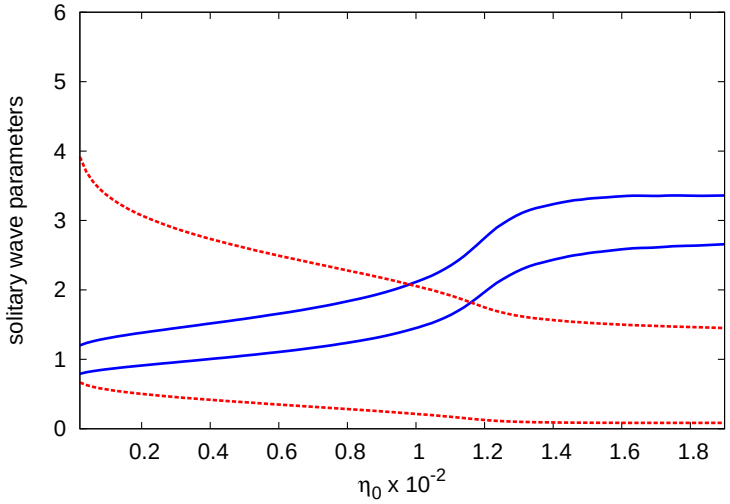

(b)

Figure 2: Variations of the solitary wave parameters in the DSW versus η_0 for (a) HS and (b) HD models. Shown are a (red upper dashed line), α (red lower dashed line), w (blue upper solid line) and β (blue lower solid line) from uniform soliton theory at $a_m = 0.5$.

but now, the upper branch in the a versus shock height a_m diagram is separated from the lower two branches. It can be seen that the results obtained for the

HD and HS models, while qualitatively similar, they vary significantly in the quantitative details. This indicates that the series (3) generates DSW which are quite different to those found by the series (2), as shown by the differences in the shock height-solitary wave amplitude response diagrams. For the geometrically appropriate HD model, S-shaped response curves occurs at much larger values of background packing fraction η_0 than for the HS model.

Figure 2 shows the solitary wave parameters a and α (amplitudes) with w and β (widths) of the uniform solitary waves in the DSW versus η_0. Shown is the uniform soliton theory given by (7) and (14). The shock height $a_m = 0.5$, for both the HS and HD models. Large amplitude solitary waves of narrow width are generated when the background packing fractions are smaller whilst for large background packing fractions, the amplitudes are smaller with broader solitary waves occurring. At $\eta_0 \approx 5.65 \times 10^{-3}$ for the HS model and $\eta_0 \approx 10.5 \times 10^{-3}$ for the HD model, the solitary wave parameters undergo a sharp variation which is associated with the existence of three solitary wave solution branches. When $\eta_0 \to 0$, the solitary wave amplitude a increases indefinitely until the model breaks down. For small η_0, the solutions obtained here are related to the upper branch of high amplitude, solitary waves.

Figure 3 shows the solitary wave amplitude, a versus the shock height a_m for the (a) HS and (b) HD (1+1)-D line DSW with the background packing fraction, $\eta_0 = 1 \times 10^{-2}$ and $k = 0$. The figures show uniform soliton theory and numerical solutions. Here, two different numerical estimates of the solitary wave amplitude are given. One estimate is the amplitude of the first solitary wave generated by the shock (the initial jump) at the z value for which this first wave has fully formed. The other estimate is the average maximum amplitude in the DSW. This approximation is obtained by taking the average between the z position at which the first solitary wave has formed and the z value where MI dominates. Here, the averaging process is needed because the largest amplitude is always changing, and the average value provides a good estimate. For this background packing fraction value, the HS model predicts a single stable solution branch, as the shock height a_m increases. For the HD model, the qualitative behaviour is different with an S-shaped response curve occurring. The solution undergoes a bifurcation at $a_m = 0.48$ at which it jumps from the low amplitude branch to the high amplitude branch. At the bifurcation point the amplitude of the solitary waves generated by the initial shock jumps from the low power to the high power stable branch, with a corresponding jump from (a,α)=$(1.56, 0.071)$ to (a,α)=$(1.85, 0.142)$. For both the HS and HD models, the comparisons are very good with errors between theory and numerics of up to 16% in the amplitude a.

Figure 4 shows the solitary wave amplitude, a versus the shock height a_m for the (a) HS and (b) HD (1+1)-D line DSW with the background packing fraction, $\eta_0 = 4 \times 10^{-3}$ and $k = 0$. Shown are the predictions of uniform soliton theory and numerical solutions. For this background packing fraction value, the HS model has an S-shaped response curve with two turning points along the curve. The bifurcation point at which the solution jumps from the lower to the upper branch is at $a_m = 0.464$, from (a,α)=$(1.45, 0.022)$ to (a,α)=$(2.34, 0.164)$.

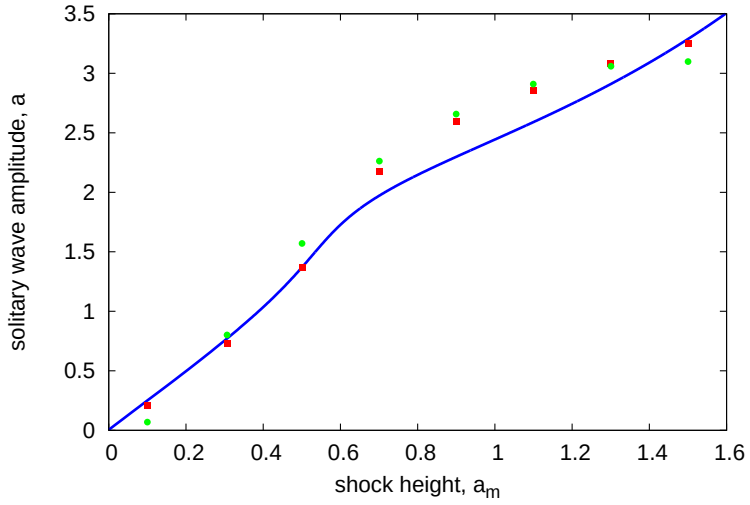

(a)

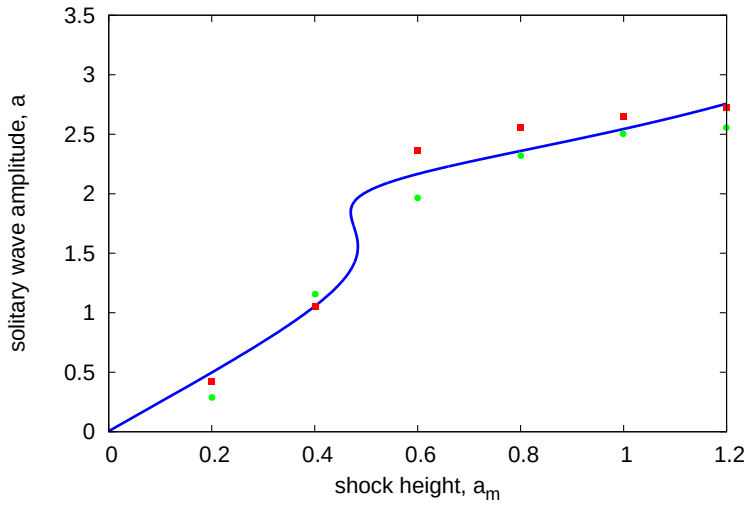

(b)

Figure 3: Solitary wave amplitude versus shock height, a versus a_m, for the (1+1)-D line DSW for (a) HS and (b) HD models. Shown are a (solid blue line) from uniform soliton theory, numerical estimates for the amplitude of the first solitary wave (red squares) and the average maximum amplitude (green circles). The other parameters are $\eta_0 = 1 \times 10^{-2}$ and $k = 0$.

However for the HD model, the upper stable branch has separated from the

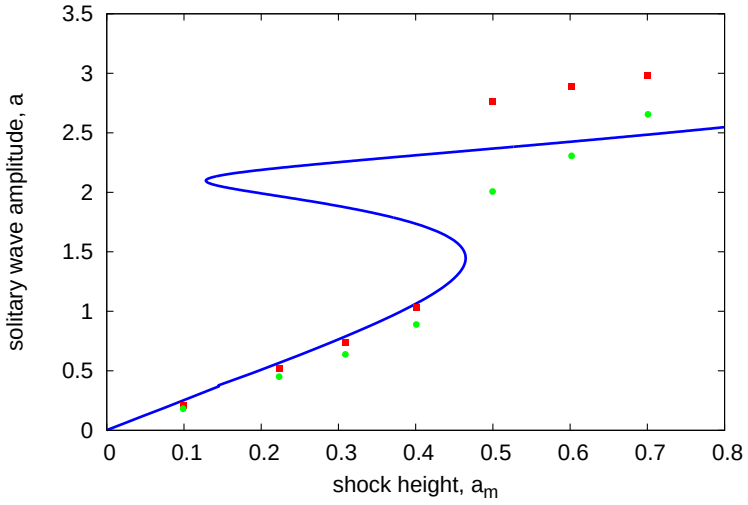

(a)

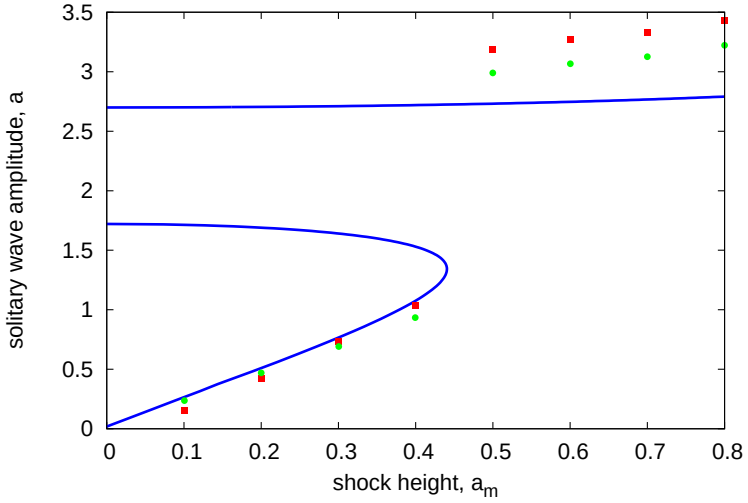

(b)

Figure 4: Solitary wave amplitude versus shock height, a versus a_m, for the (1+1)-D line DSW for (a) HS and (b) HD models. Shown are a (solid blue line) from uniform soliton theory, numerical estimates for the amplitude of the first solitary wave (red squares) and the average maximum amplitude (green circles). The other parameters are $\eta_0 = 4 \times 10^{-3}$ and $k = 0$.

middle unstable branch. The jump occurs at $a_m = 0.44$ from (a,α)=(1.35, 0.018)

to $(a,\alpha)=(2.72, 0.413)$. This bistable behaviour is related to the bistable power versus propagation constant curves, for low background packing fraction, as shown in figures 1 and 4[6]. There is a good comparison between the theory and the numerical solutions with a maximum 16% error occurring for the range of the shock height values shown on the figure. The errors are higher on the upper branch as the wave amplitudes are higher there. The difference in the value of a_m at which the bifurcation occurs for the HS and HD models is very small with a 5% difference. The theoretical and numerical solutions for both colloids are quite similar before the jump, but the estimates start to differ on the upper branches.

Figure 5 shows the solitary wave amplitude, a versus the shock height a_m for the (a) HS and (b) HD (1+1)-D line DSW with background packing fraction $\eta_0 = 1 \times 10^{-3}$ and $k = 0$. Shown are the predictions of uniform soliton theory and numerical solutions. For this lower value of background packing fraction, both the HS and HD models have upper stable branches that have separated from the unstable branch. This separation happens because the jump amplitude a_m for the missing portion of the S-shaped curve has negative values. For the HS model, the bifurcation point at which the jump occurs is at $a_m = 0.42$. The jump is from $(a,\alpha)=(1.35, 4.89 \times 10^{-3})$ to $(a,\alpha)=(3.19, 0.307)$. For the HD model, the bifurcation point is at $a_m = 0.41$ with the jump from $(a,\alpha)=(1.34, 4.89 \times 10^{-3})$ to $(a,\alpha)=(3.35, 0.564)$. The difference in the HS and HD bifurcation points is very small, being only 2%. The amplitude of the flat upper branches for the HS and HD models have a variation up to 7% at $a_m = 0.8$. There exists a good comparison between the semi-analytical and the numerical solutions of the HS and HD models with errors of less than 10% on the lower branch and about 20% error on the upper branch.

Figure 6 shows the numerical solution for $|u|$ versus x for the (1+1)-D line DSW for both the (a) HS and (b) HD models at $z = 1100$. The initial and background packing fractions are $\eta_0 = 1 \times 10^{-2}$ and $\eta_m = 1.29 \times 10^{-2}$. For the HS model, two solitary waves have formed where the leading edge occurs at $x = -48.5$ and the highest peak is $a = 0.95$. The first HS solitary wave has a maximum amplitude $a = 1.59$, which forms at a slightly shorter length of $z = 920$. Between $z = 920$ and $z = 1100$ a second wave forms, which can interact with the first wave, causing the amplitudes to vary. The uniform soliton theory predicts a solitary wave amplitude of $a = 1.51$ and $\alpha = 0.05$ which is quite close to the numerical value with less than 5% error. For the HD model at $z = 1100$, the first solitary wave has developed to its maximum amplitude $a = 1.33$. Uniform soliton theory predicts $a = 1.37$ and $\alpha = 0.043$ which is again close to the numerical value with less than 3% error.

For both HS and HD models we can see the differences between the semi-analytical solutions and numerical predictions for the solitary wave amplitudes are very small. We do not show the packing fraction η_m because it has the same profile as $|u|$. For the HS model, the solitary waves will have a higher maximum amplitude, which occurs at a smaller value of z.

Figure 7 shows the numerical solution for $|u|$ versus x for the (1+1)-D line DSW for both the (a) HS and (b) HD models at $z = 2500$. The initial and back-

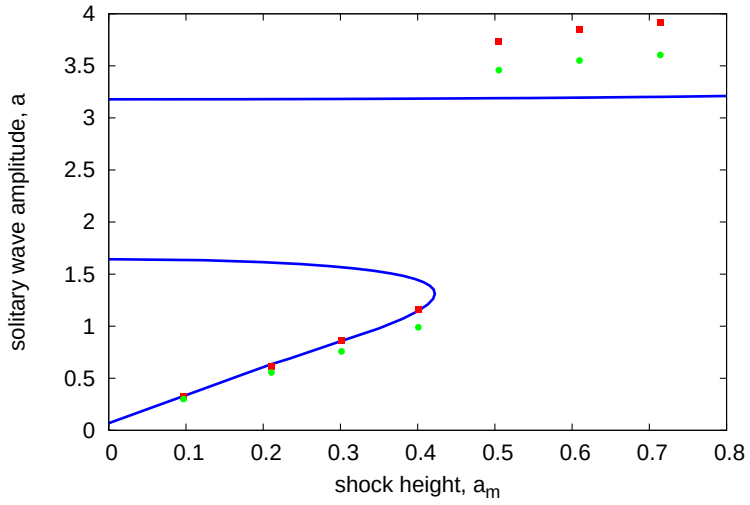

(a)

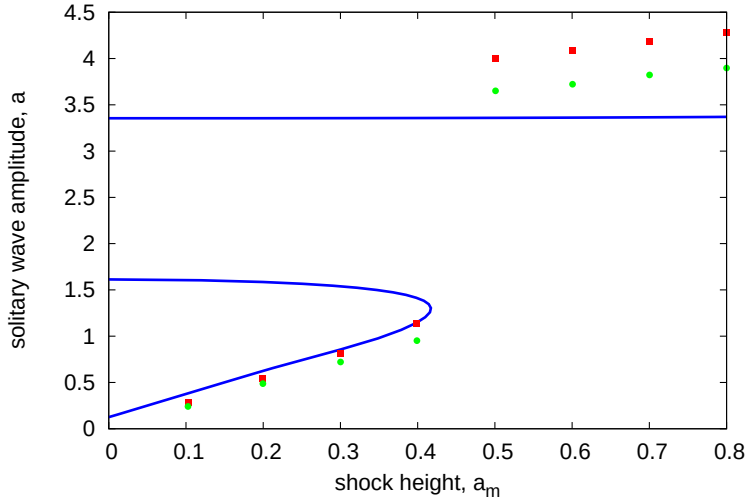

(b)

Figure 5: Solitary wave amplitude versus shock height, a versus a_m, for the (1+1)-D line DSW for (a) HS and (b) HD models. Shown are a (solid blue line) from uniform soliton theory, numerical estimates for the amplitude of the first solitary wave (red squares) and the average maximum amplitude (green circles). The other parameters are $\eta_0 = 1 \times 10^{-3}$ and $k = 0$.

ground packing fractions are $\eta_0 = 1 \times 10^{-2}$ and $\eta_m = 1.29 \times 10^{-2}$ respectively.

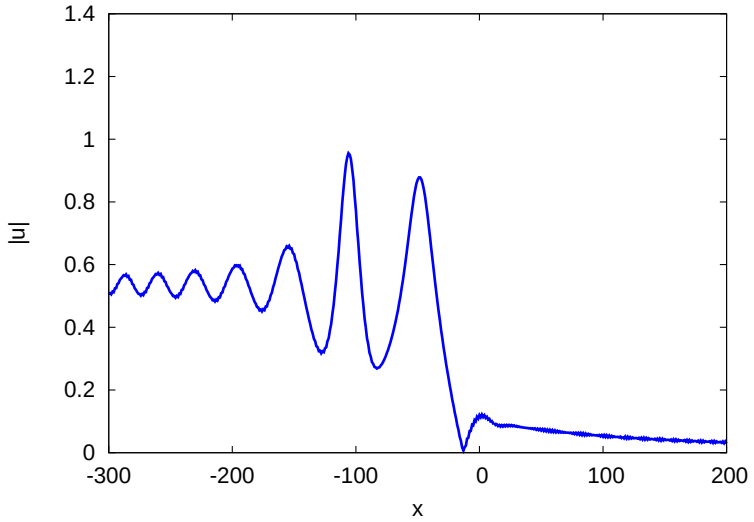

(a)

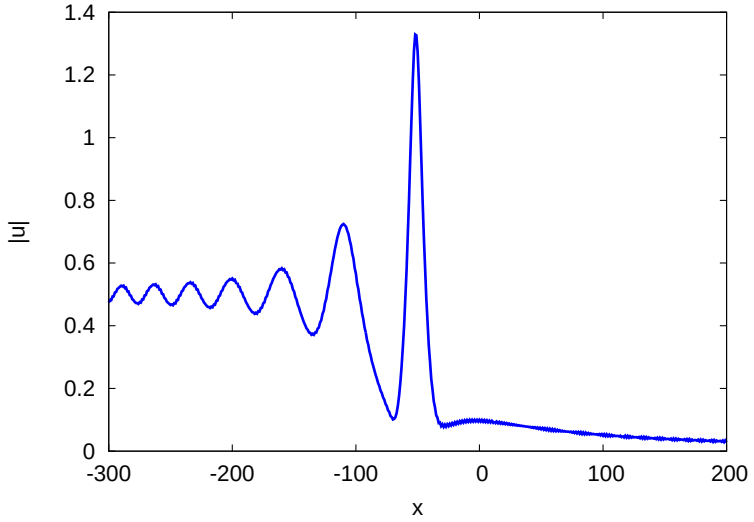

(b)

Figure 6: The electric field amplitude $|u|$ versus x for the (1+1)-D line DSW. Shown are the numerical solutions for (a) HS and (b) HD at $z = 1100$. The initial and background packing fractions are $\eta_0 = 1\times10^{-2}$ and $\eta_m = 1.29\times10^{-2}$.

For a DSW described by a hyperbolic system of modulation equations, the DSW consists of an expansion fan. Here, as the modulation equations form an elliptic system and there is no hyperbolic expansion fan, the individual waves do not

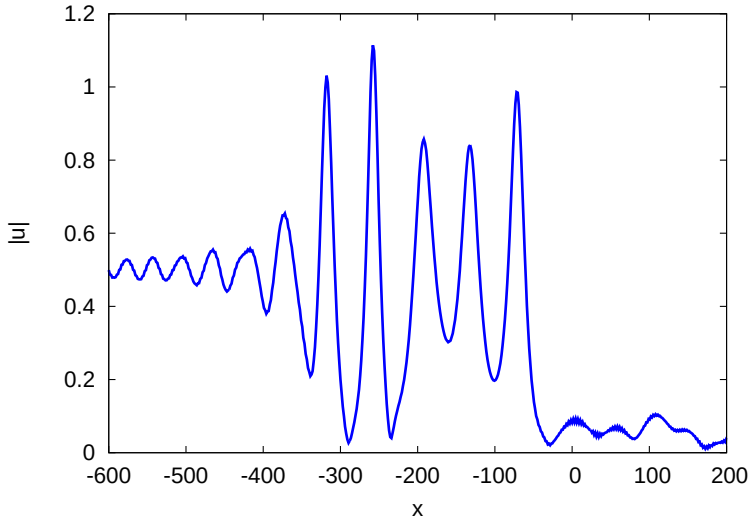

(a)

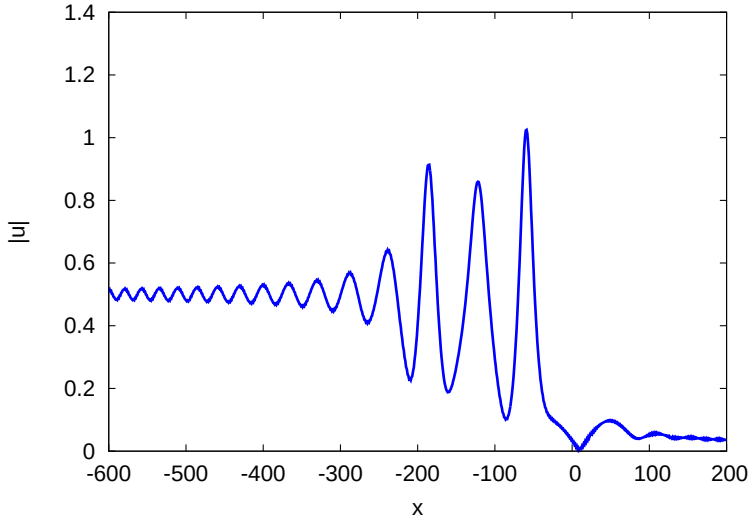

(b)

Figure 7: The electric field amplitude $|u|$ versus x for the (1+1)-D line DSW. Shown are the numerical solutions at the initial jump for (a) HS and (b) HD at $z = 2500$. The initial and background packing fractions are $\eta_0 = 1 \times 10^{-2}$ and $\eta_m = 1.29 \times 10^{-2}$.

completely separate[16, 17]. Hence, the waves continue to interact with each other and they are not ordered by amplitude. For the HS model, there are five

solitary waves formed where the fourth wave is the largest with $a = 1.11$. The maximum amplitude in the DSW, averaged over z is 1.09. The semi-analytical solitary wave for the HS model has amplitude $a = 1.51$ hence, the comparison between the semi-analytical solutions and numerical predictions differs by 26%. For the HD model, only three solitary waves have formed where the leading edge solitary wave is the largest, with maximum amplitude of $a = 1.02$. The maximum amplitude in the DSW, averaged over z is $a = 0.94$. The semi-analytical solitary wave for the HS model has amplitude $a = 1.37$ hence, the comparison between the semi-analytical solutions and numerical predictions differ by 31%. The HS model predicts larger solitary waves amplitudes than the HD model.

4.2 Temperature dependent model

We now consider the HD model but with a temperature dependent second virial coefficient given by (3) where $B_2 = 2 - \frac{100}{T}$ and $B_2 \to 2$, the HD case, as the temperature becomes large. This form of the second virial coefficient allows us to consider temperature dependent effects on the formation and structure of DSW.

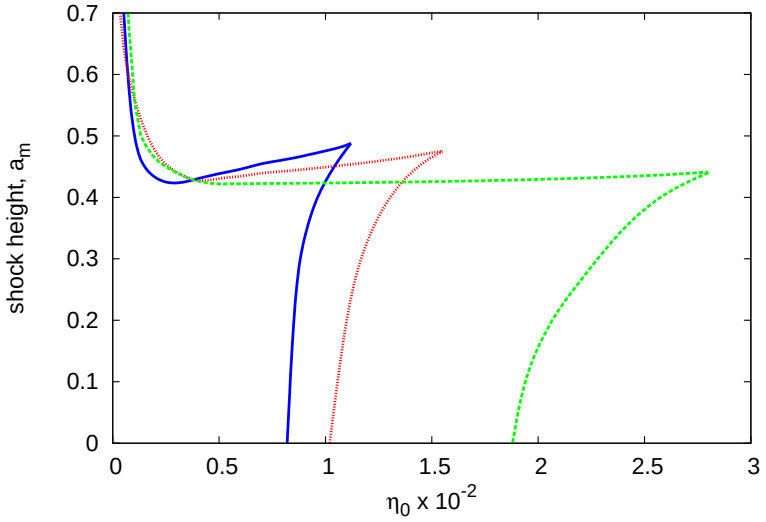

Figure 8: The dispersive shock height, a_m, at the bifurcation point versus the background packing fraction η_0 for the (1+1)-D line DSW. Shown are $T = 50$ (dashed green line), $T = 100$ (red dotted line) and $T = 500$ (solid blue line).

Figure 8 shows the dispersive shock height, a_m at the bifurcation points versus the background packing fraction η_0 for the temperature dependent (1+1)-D line DSW. Three cases, $T = 50, 100$, and 500 of the uniform soliton theory are shown. For $T = 50$, bifurcation points exists for $\eta_0 < 2.8 \times 10^{-2}$, while for $T = 100$ and $T = 500$, bifurcation points exist for $\eta_0 < 1.55 \times 10^{-2}$ and

$\eta_0 < 1.12 \times 10^{-2}$ respectively. So, as temperature increases, the region of parameter space in which multiple steady-state solutions decreases, and the S-shaped response curve occurs only at lower values of η_0. A single, stable, a versus a_m solution branch will occur beyond these bifurcation points; these are the parameter values that separates the bi-stable and mono-stable regimes for the solitary wave solution of the (1+1)-D temperature dependent model. We see three solution branches (two stable, one unstable) when η_0 is less than the critical values mentioned above. As the temperature increases, the HD model limit is approached, for which the bifurcation points occur when $\eta_0 < 1.05 \times 10^{-2}$.

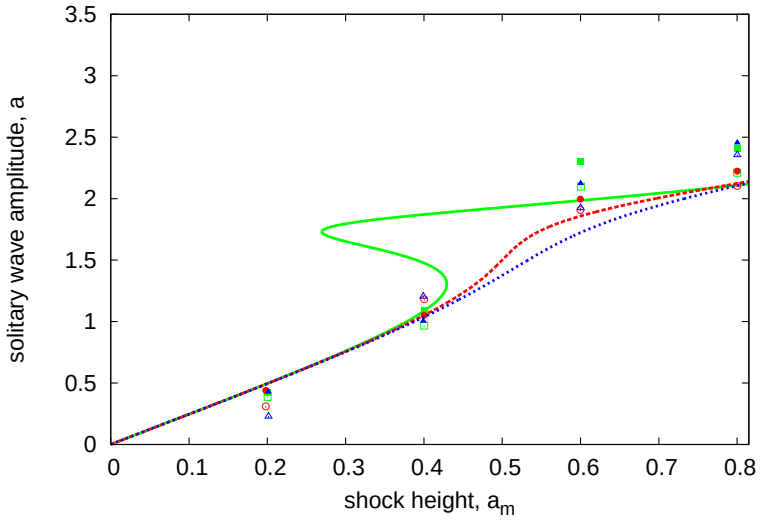

Figure 9: Solitary wave amplitude versus shock height, a versus a_m, for the temperature dependent line DSW. Shown are the uniform solitary theory for $T = 50$ (solid green line), $T = 100$ (dashed red line) and $T = 500$ (dotted blue line), numerical estimates for $T = 50$ (green squares), $T = 100$ (red circles) and $T = 500$ (blue triangles) for the first solitary wave and average maximum amplitude for $T = 50$ (green hollow squares), $T = 100$ (red hollow circles) and $T = 500$ (blue hollow triangles). The other parameters are $\eta_0 = 2 \times 10^{-2}$ and $k = 0$.

Figure 9 shows the solitary wave amplitude versus the shock height, a versus a_m for the temperature dependent line DSW for $T = 50$, $T = 100$ and $T = 500$ with the background packing fraction, $\eta_0 = 2 \times 10^{-2}$ and $k = 0$. Shown is the predictions of uniform soliton theory and numerical solutions. An S-shaped curve exists for $T = 50$, and unique curves for $T = 100$ and $T = 500$. The S-shaped response curve disappears at $T \approx 90$. For $T = 50$, the bifurcation point occurs at $a_m = 0.43$ and the amplitude jumps from $(a, \alpha) = (1.31, 0.08)$ to $(a, \alpha) = (1.89, 0.39)$. For $T = 100$ and $T = 500$, single solution branches

exist. This figure illustrates that temperature variations can have a dramatic effect on the solitary wave amplitude in the DSW. For low temperatures, a bifurcation point exists, at which a significant jump in solitary wave amplitude can occur. However at high temperatures this bifurcation in amplitude does not occur. There is a good comparison between the theoretical solutions and numerical estimates over the range of the graph, with is a maximum error of up to 19%. The curve for $T = 500$ is very close to the HD model with a maximum of 1% difference in the curve.

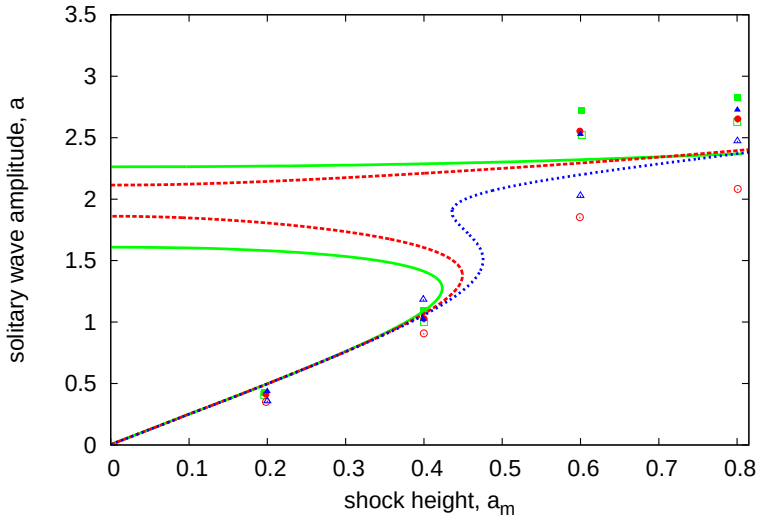

Figure 10: Solitary wave amplitude versus shock height, a versus a_m, for the temperature dependent line DSW. Shown are the uniform solitary theory for $T = 50$ (solid green line), $T = 100$ (dashed red line) and $T = 500$ (dotted blue line), numerical estimates for $T = 50$ (green squares), $T = 100$ (red circles) and $T = 500$ (blue triangles) for the first solitary wave and average maximum amplitude for $T = 50$ (green hollow squares), $T = 100$ (red hollow circles) and $T = 500$ (blue hollow triangles). The other parameters are $\eta_0 = 1 \times 10^{-2}$ and $k = 0$.

Figure 10 shows the solitary wave amplitude versus the shock height, a versus a_m for the temperature dependent line DSW at $T = 50$, $T = 100$ and $T = 500$ with the background packing fraction, $\eta_0 = 1 \times 10^{-2}$ and $k = 0$. The figure shows uniform soliton theory and numerical solutions. Multiple solution branches exist for all temperatures except that the upper stable branches are separated from the middle unstable branch for $T = 50$ and $T = 100$. The S-shaped curves become separated at around $T \approx 120$. For $T = 50$, the bifurcation point at which the jump from the lower to the upper branch occurs is at $a_m = 0.42$, from $(a,\alpha)=(1.28, 0.04)$ to $(a,\alpha)=(2.29, 0.54)$. For $T = 100$, the bifurcation point occurs at $a_m = 0.46$ and the jump occurs at $(a,\alpha)=(1.38, 0.05)$

to $(a,\alpha)=(2.23, 0.36)$. For $T = 500$, the bifurcation point occurs at $a_m = 0.48$ and the jump occurs at $(a,\alpha)=(1.51, 0.06)$ to $(a,\alpha)=(2.06, 0.22)$. We can see here that as temperature increases, the bifurcation point also increases in magnitude. These results show excellent comparisons between the theoretical solutions and numerical estimates.

Figure 11 shows the numerical solution for $|u|$ versus x for the temperature dependent line DSW with $T = 50$ and $T = 100$. The initial packing fraction is $\eta_m = 1.27 \times 10^{-2}$ and the background packing fraction $\eta_0 = 1 \times 10^{-2}$. (a) shows the z values at which the first wave has fully formed. For $T = 50$, the first wave has fully formed at $z = 975$ while for $T = 100$, the wave has fully formed at $z = 1085$. (b) shows the result at z=1200 where the properties of the waves start to differ. The first solitary wave in (b) has developed to its maximum height at $a = 2.28$ for $T = 50$ and $a = 1.65$ for $T = 100$. Here we can see that as temperature increases, the maximum height for the solitary wave decreases. We then consider a longer propagation distance as shown in (c) where $z = 2500$ and we can see that a bore has formed with four solitary waves for both models, but with significantly different maximum amplitude. The leading wave is the largest with $a = 2.32$ for $T = 50$ and $a = 1.33$ for $T = 100$. Again, the maximum height for the largest solitary wave decreases when temperature increases. The average maximum amplitude is $a = 1.55$ and $a = 0.97$ for $T = 50$ and $T = 100$, respectively, with corresponding semi-analytical solutions of $a = 1.31$ and $a = 1.24$. Thus, the differences between the semi-analytical solutions and the numerical predictions are 15% and 22%, for $T = 50$ and $T = 100$, respectively.

5 Conclusions

This paper combines semi-analytical solutions for colloidal solitary waves and uniform soliton theory to predict the amplitude of solitary waves that form in colloidal dispersive shock waves. The governing equations are formulated using a series for the non-ideal gas law with hard sphere, hard disk and temperature dependent models all considered. The approximation for the solitary wave amplitudes is found to give good to excellent comparisons with numerical estimates. Three qualitatively different solitary wave amplitude versus jump height diagrams are obtained depending on the value of background packing fraction. When the background packing fraction is small, the upper solution branch separates from the middle unstable branch. At moderate values, we obtain an S-shaped response curve results, with multiple solution branches. For large background packing fractions, a single stable solution branch occur. The temperature dependent model results in changes to the parameter space, in which multiple solutions branches occur. From this semi-analytical theory, the critical background packing fractions at which multi-stability is lost are well predicted and changes in temperature are shown to effect the bifurcation patterns and the turning points.

It is hoped that this theoretical study will encourage experimental investig-

ations of colloidal dispersive shock waves and temperature dependent particle interaction effects. The model and semi-analytical solutions developed here could be easily used by experimental groups simply by selecting appropriate virial coefficients, which correspond to their experimental colloidal medium. Hence we believe that the colloidal model equations and solutions presented here provide an extremely useful testbed for exploring different colloidal media and particle interaction models.

References

[1] W. Wan, D. V. Dylov, C. Barsi, and J. W. Fleischer, Diffraction from an edge in a self-focusing medium, *Opt. Lett.*, **35** (2010) 2819.

[2] M. Peccianti, C. Conti, and G. Assanto, Optical modulational instability in a non-local medium, *Phy. Rev. E*, **68** (2003) 025602.

[3] G. Assanto, T. R. Marchant, and N. F. Smyth, Collisionless shock resolution in nematic liquid crystals, *Phy. Rev. A*, **78** (2008) 063808.

[4] T.R. Marchant and N.F. Smyth, Semi analytical solutions for dispersive shock waves in colloidal media, *J. Phys. B: At. Mol. Opt.*, **45** (2012) 145401.

[5] J. Tian and Y. Gui, Equations of state for fluids: empirical temperature dependence of the second virial coefficient, *J. Phys. Chem. B*, **111** (2007) 10970.

[6] A. Azmi and T.R Marchant, Colloidal solitary waves with temperature dependent compressibility, *J. Opt.*, **16** (2014) 055203.

[7] M. Matuszewski, W. Krolikowski, and Y.S. Kivshar, Spatial solitons and light-induced instabilities in colloidal media, *Opt. Express*, **16** (2008) 1371.

[8] J. Tian, H. Jiang, Y. Gui, and A. Mulero, Equation of state for hard-sphere fluids offering accurate virial coefficients, *Phys. Chem: Chem. Phys.*, **11** (2008) 11213.

[9] A. Santos, M. Lopez de Haro, and S.B. Yuste. An accurate and simple equation of state for hard disks, *J. Chem. Phys*, **103** (1995) 4622.

[10] W.L. Kath and N.F. Smyth, Soliton evolution and radiation loss for the nonlinear Schrödinger equation, *Phys. Rev. E*, **51** (1995) 1484.

[11] R.H.J Grimshaw and N.F. Smyth, Resonant flow of a stratified fluid over topography, *J. Fluid Mech.*, **169** (1986) 429.

[12] T.R. Marchant and N.F. Smyth, Approximate techniques for dispersive shock wave in nonlinear media, *J. Nonlinear Opt. Phys.*, **21** (2012) 1250035.

[13] T.R. Marchant and N.F. Smyth, Solitary waves and their stability in colloidal media: Semi-analytical solutions, *Dyn. Cont. Disc. Imp. Sys. B*, **19** (2012) 525.

[14] T. R. Marchant and B. Liu, The steady-state microwave heating of slabs with small Arrhenius absorptivity, *J. Engng. Math.*, **33** (1998) 219.

[15] B. Liu and T.R. Marchant, Microwave heating of two-dimensional slabs with small Arrhenius absorptivity, *IMA J. Appl. Math.*, **62** (1999) 137–166.

[16] G. A. El, A. V. Gurevich, V. V. Khodorovskii, and A. L. Krylov, Modulational instability and formation of a nonlinear oscillatory structure in a focusing medium, *Phys. Lett. A*, **177** (1993) 257.

[17] A.M. Kamchatnov, S.A. Darmanyan, and F. Lederer, Formation of solitons on the sharp front of the pulse in an optical fiber, *Phys. Lett. A*, **245** (1998) 259.

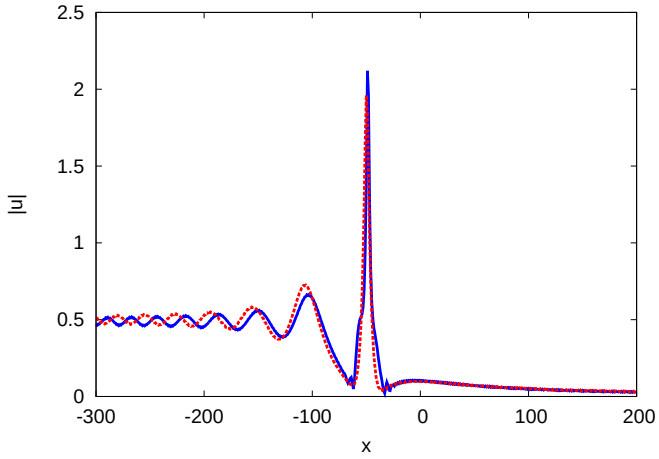

(a)

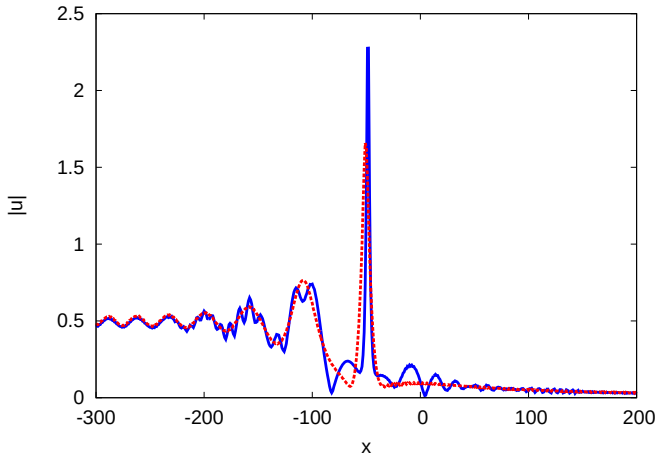

(b)

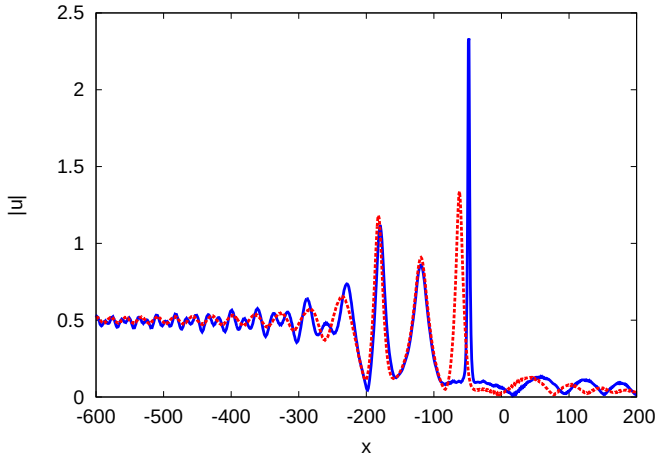

(c)

Figure 11: The electric field amplitude $|u|$ versus x for the temperature dependent line DSW. Shown are the numerical solutions at (a) the z values at which the first wave has fully formed (b) $z = 1200$ and (c) $z = 2500$ for temperature dependent models $T = 50$ (solid blue line) and $T = 100$ (dashed red line). The other parameters are $\eta_0 = 1 \times 10^{-2}$ and $\eta_m = 1.27 \times 10^{-2}$.